# Surface formation mechanism in waterjet guided laser cutting of a Ni-based superalloy

Zhirong Liao [a], Dongdong Xu [a], Dragos Axinte [a]*(1), Jeremie Diboine [b], Anders Wretland [c]

*a Faculty of Engineering, University of Nottingham, UK*
*b Synova S.A., Switzerland*
*c GKN Aerospace Engine Systems, Sweden*

Waterjet guided laser (WJGL) cutting is a relatively new technology for high-precision machining of difficult-to-cut materials. However, its material removal mechanism presents some unique features because of the interaction between laser, waterjet and workpiece. This paper investigates the surface formation mechanism in WJGL cutting of Ni-based superalloy and its influence on the fatigue performance. Two different microstructures have been found on the surface layer, i.e. recast crystals and redeposited amorphous oxide, resulting from solidification of melt and plasma respectively under the laser-waterjet interaction. Mechanical twinning structures were also revealed in the substrate due to the waterjet confined plasma shockwave impact.

Laser, Cutting, Surface integrity

## 1. Introduction

Laser cutting has been considered as a promising method to machine a wide range of different materials, especially for difficult-to-cut metals, e.g. Ni-based superalloy. However, due to the nature of defocus and heat dissipation into the workpiece, the conventional laser cutting (CLC) of metals usually leads to extensive metallurgical surface defects as well as inclined kerf [1, 2]. Waterjet guided laser (WJGL) machining, by using a waterjet beam to guide the laser like a glass fibre, can achieve a more accurate cutting with high quality kerf walls under a dramatically increased working distance, e.g. 25-100 mm [3]. Moreover, the waterjet can also minimise the undesired thermal effect by continuously cooling the sample during the cutting process and so to reduce the surface damage [4].

Different from conventional mechanical machining of Ni-based superalloy where the surface damage is induced by thermal-mechanical effect [5], laser machining mainly introduces thermal damages, i.e. white layer (WL) [6]. In general, WL is not preferable in safety-critical industry applications due to the deterioration of workpiece fatigue life. Hence, investigating the formation mechanism of this layer represents a crucial aspect from both academic and industrial points of view. However, while the WL formation mechanism in CLC of Ni-based superalloy has been revealed, i.e. through remelted crystals [6], the surface metallurgical changes in WJGL, whereby the presence of waterjet complicates the material removal mechanism, remains unclear.

In this respect, this paper investigated the surface formation mechanism in WJGL cutting of a Ni-based superalloy. Due to the small thickness of the surface defects, i.e. under tens of micrometres, advanced material investigation methods, e.g. electron backscatter diffraction (EBSD), transmission Kikuchi diffraction (TKD), scanning transmission electron microscopy (STEM), energy dispersive X-ray (EDX) mapping were employed to understand the phenomena governing the material microstructural evolution during the WJGL cutting process. The fatigue performance was further investigated to understand the influence of the surface defects on part functional performance.

## 2. Material removal through waterjet guided laser (WJGL)

In WJGL the laser beam is focused into a waterjet nozzle and guided by a laminar waterjet where it undergoes total internal reflection at the water/air boundary, leading to a long working distance without the beam defocusing (Fig. 1). In this scenario, while the material removal is dominated by the laser ablation through the formation of the melt pool, vapour and plasma plume, the waterjet, with its high heat capacity, can significantly influence the thermodynamics and kinetics of the ablated matter, providing good heat management as well as cleaning of debris from the work zone. Hence, compared to the laser ablation in air, whereby a great proportion of the heat penetrates into a deep bulk area (e.g. >1mm) and yields drastic thermal effects, the WJGL process, however, provides a smooth cut and localised heat influence.

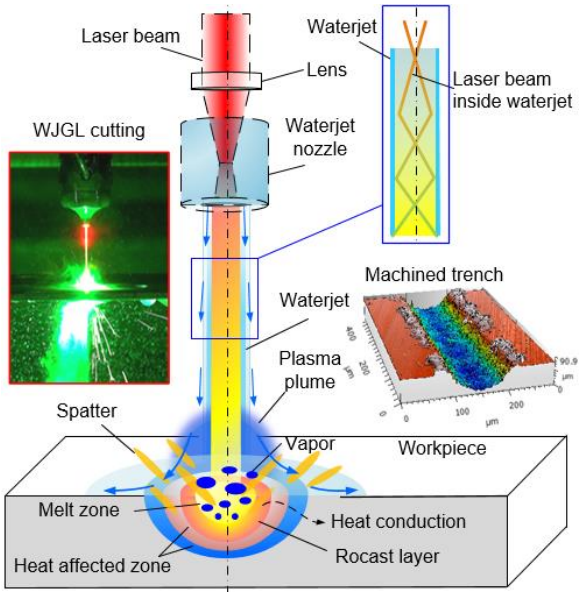


**Fig. 1.** Material removal principle through waterjet guided laser machining

## 3. Experimental setup

To investigate the surface formation mechanism of WJGL cutting of a Ni-based superalloy and, further, to evaluate its influence on functional performance, e.g. fatigue life, an Inconel 718 plate was cut into a dimension of 100 mm × 6mm × 6 mm by WJGL machine (Synova MCS 300). The waterjet (diameter of 50 μm) was pumped with a pressure of 40 MPa and the laser was a Nd:YAG pulsed laser at 532 nm with an average power of 90 W, frequency of 12 kHz, 250 ns pulse duration (1.5 GW/cm$^2$). The samples were cut at a feed rate of 120 mm/min pre-optimised for roughing and SoD of 10 mm through multilayer (i.e. 14 passes) cutting. The residual stress and crystallography evolution of the surface layer have been investigated, wherein the microstructure alteration represents the specific mechanism of laser-waterjet-workpiece interactions. Four points bending fatigue test was also conducted under sinusoidal cyclic loading stress at the level of 60% -140% of the yield stress (1250MPa) with a frequency of 5 Hz and 0.1 stress amplitude ratio.

## 4. Surface formation mechanism in WJGL cutting

### *4.1. Surface integrity of WJGL cut Ni-based superalloy*

In general, from the top surface observation of the WJGL cut Inconel 718 only recast layer can be observed (Fig. 2a), which are formed through the solidification of melt. Specifically, from Fig. 2b it can be seen that due to the waterjet stream flushing the recast material is aligned in a ridged-like features along the waterjet flow direction. This indicates that, although the workpiece material is ablated by laser beam, the waterjet plays an important role on the morphology of workpiece surface formation.

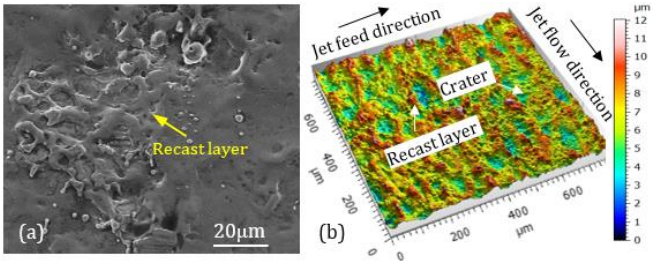


**Fig. 2.** WJGL cut surface: (a) SEM observation and (b) 3D morphology

A polished and etched cross-sectional SEM image of the WJGL cut surface (Fig. 3a) shows a loose white layer with a thickness of ~8 μm. Different from conventional laser cut Ni-based superalloys whereby a large heat affected zone (HAZ) usually appears [6], for WJGL cut surfaces there is no clear HAZ observed. This is because most heat in the ablation area has been absorbed by the waterjet during the inter-pulse period, which reduces the heat transfer and accumulation in the substrate.

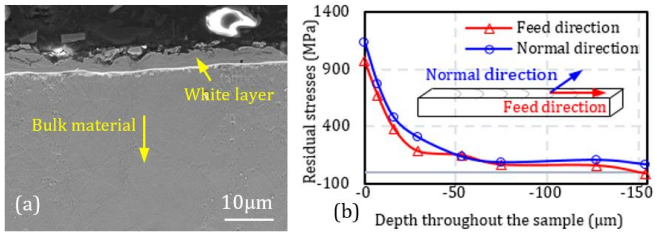


**Fig. 3.** (a) SEM image of cross section and (b) residual stress profile

A specific residual stress examination through XRD (Fig. 3b) shows high tensile residual stresses (~1100 MPa) at the top surface while decreases significantly at a depth about 50 μm in the substrate. This tensile stress is attributed to the remelt quenching that leads to shrinkage of the superficial layer. However, the influenced depth is much reduced (i.e. 50 um) compared to conventional laser cutting. This can be explained by the pulse to pulse heat accumulation in the substrate in CLC compared to the inter-pulse cooling by the waterjet in WJGL.

### *4.2. Specifics of white layer formation mechanism in WJGL cutting*

From the metallurgical observations the mechanism of white layer formation is not evident. Consequently, ion channelling contrast (ICC) and TKD imaging were conducted in the superficial layer for further investigation, as shown in Fig. 4. It can be clearly observed from ICC image that there are mainly two different microstructures/contrasts in the white layer, i.e. recast (including also recast droplet and spatter) and redeposited material. The recast is generated from the solidified melt while the redeposition originates from the deposition of the vapour/plasma plume. A further observation from TKD (Fig. 4 b and c) shows the epitaxial grown polycrystalline structure of recast material. This demonstrates that the heat energy in the melting pool is sufficient to facilitate the crystalline growth. There are also some nano particles within the recast material showing the same contrast as redeposited material. A thin redeposited film is adhered to the recast layer with relatively small bonding force and forms several cracks/splits under thermal stress (Fig. 4a). The TKD band contrast image (Fig. 4b) shows that this layer is with amorphous structure and cannot be indexed. A further EDX mapping (Fig. 4d) demonstrates that the redeposition is mainly formed by oxide while the recast presents the same elemental compositions as the substrate due to its nature of solidified melt.

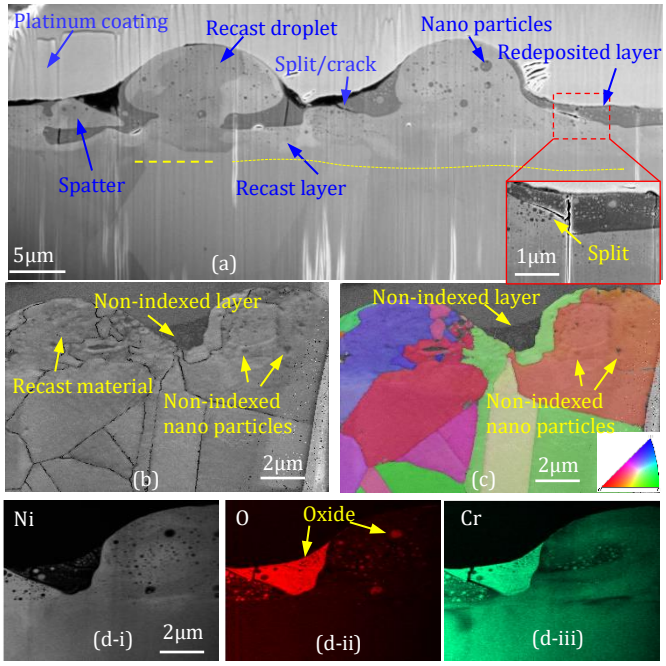


**Fig. 4.** The cross-section of recast layer: (a) ICC, (b) band contrast and (c) inverse pole figure (IPF) of TKD, (d) EDX mapping.

A further observation on a cross section of spatter area was also scanned under EBSD to understand the crystallographic nature of this layer (Fig. 5). It is interesting to see that the redeposition is "wrapped" by a spatter which was ejected from the explosive melt. Nevertheless, the spatter area is featured with small grains (Fig. 5d) while the common recast layer (Fig. 4c) presents large grain structure connected to the substrate. The small grain size of spatter is possibly due to the fast cooling (i.e. quenching) from the external water that restricts its grain growth during ejection.

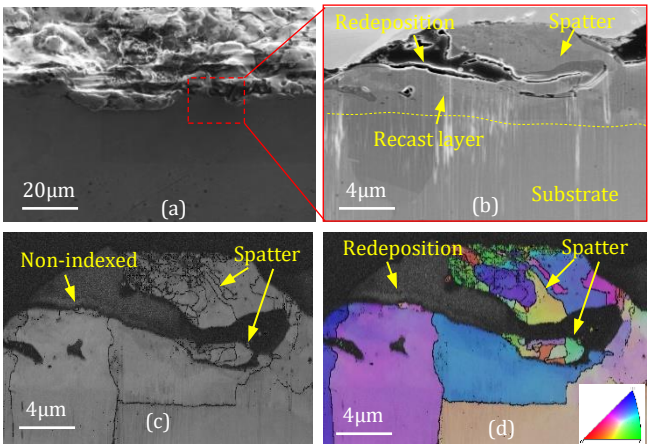

**Fig. 5.** The cross-section of spatter area: (a) and (b) SEM observation, (c) band contrast and (d) IPF of EBSD mapping.

Therefore, based on the above observations it can be concluded that the WJGL cut surface is formed with two mechanisms: melt and vapour/plasma plume. In this context, the recast layer is formed through the solidification of melt under waterjet cooling whereby the accompanied explosive boiling melt and ejected droplets forms also the spatter and recast droplets. The vapour/plasma plume on the contrary generates a thin redeposition film which mainly contains highly oxidised amorphous structure. In this scenario, the expansion and movement of the plasma plume are confined by the waterjet due to its higher density and viscosity, hence can be easily oxidised and deposited on to the top surface forming a thin film. This is different from the conventional laser ablation where the vapour/plasma plume usually dissipates in air.

These two different microstructures are manifested on the dark field STEM observation (Fig. 6a), whereby the redeposited layer is demonstrated as a thin coating film (~500nm) on the top of the thick (~3 μm) recast layer. High density dislocation tangles (Fig. 6b) are also found in the recast layer due to the fast cooling rate that brings lattice migration during the solidification. A mass of nano grains are present within the recast layer (Fig. 6c and d), which are corresponding to the nano-oxide particles in Fig. 4. These nano grains embedded in the recast material originate from the solidification of the vaporised matter in the boiling melt pool under waterjet cooling. More interestingly, an agglomeration of δ phase is also observed beneath the recast layer (Fig. 6a) which was transformed from over-aged γ'' phase, indicating that the substrate suffered a high temperature (>650 °C) near the melt pool.

Another extraordinary phenomenon is that high density mechanical twins (MTs) present in the superficial layer after WJGL cutting. These mechanical twins were most likely generated from the high-pressure plasma shockwaves that impacts on the surface due to the partial confinement by dynamic waterjet. Such a significant "mechanical effect" is not often observed in conventional laser machining where the plasma plume is not confined. Furthermore, these mechanical twins show a high density near the top surface and decreases towards the substrate, indicating a pressure gradient from the confined plasma plume downwards the substrate. More interestingly, submicron rhombic blocks are also present, which are formed through the intersection of various MTs aligned in different directions subjected to multiple shock impacts that is induced by high frequency pulse laser. These microstructures indicate that a secondary effect in WJGL cutting, i.e. laser shock penning, that can lead to material strengthening.

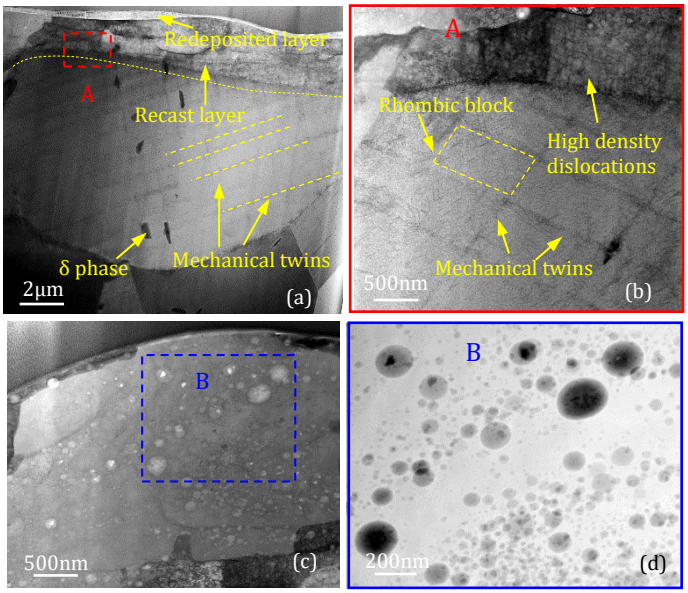


**Fig 6.** STEM of recast layer: (a)-(c) Dark field and (d) HAADF observations

A high magnification STEM observation on the redeposited film shows that this layer is composed of both amorphous and nanocrystalline structure, as shown in Fig. 7(a) and (b). While this amorphous layer is mainly structured as a stable oxide film (with oxyphilic elements, e.g. Cr, Nb and Ti), the nanograins in this layer are composed of γ element, i.e. Ni, as shown in Fig. 7 (c). In this scenario, due to the waterjet confinement, the thermodynamic and kinetic properties of the plasma can be greatly restricted; hence, the supplied vaporised mass cannot further evolve to plasma but condensed to nanograins and enfolded into the redeposited film. On the other hand, the amorphous oxide layer presents a high brittleness and can easily generates microcracks (Fig. 7b) under thermal stress while only high density dislocation tangles are observed in the underlying recast layer (Fig. 7 a).

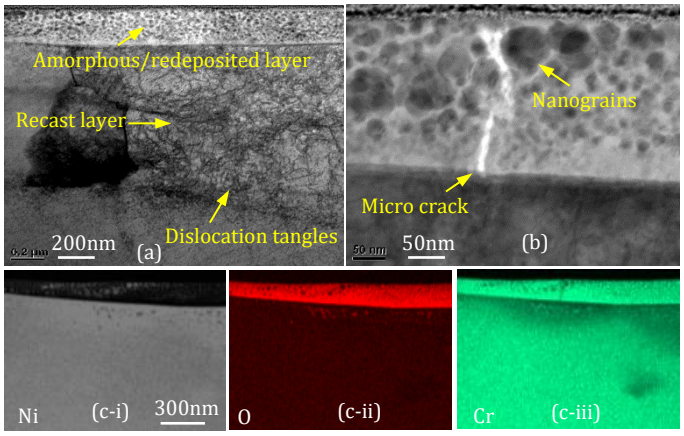


**Fig 7.** Microstructure of redeposited layer: (a) and (b) STEM, (c) EDX

Based on above observations, the surface layer formation mechanism of WJGL cutting can be explained with the following stages (Fig.8, Inconel 718 as an example): (I) the laser beam is transmitted through a laminar waterjet and irradiates the material leading to melting, vaporisation and eventually ionisation; (II) due to its higher density and viscosity the waterjet can partially confine the expansion of plasma plume. The partially confined plasma can react with the dissolved gases and redox equivalents from the water/atmosphere and leads to the formation of oxide; (III) the confined plasma plume/oxide are then deposited on the top

surface layer under a fast cooling rate with water cooling, and eventually forms an amorphous structure accompanied with γ nanograins which are solidified from vapour; (IV) in the meantime, due to the water confinement, the expanded high pressure plasma plume generates a shockwave impact on the substrate and forms mechanical twins; (V) as most heat conduction has been predominantly absorbed by waterjet, the remaining melt solidifies quickly and forms recast layer; (VI) a transformation of over-aged γ'' to δ phase also occurs beneath the recast layer due to the temperature gradient near the melt pool.

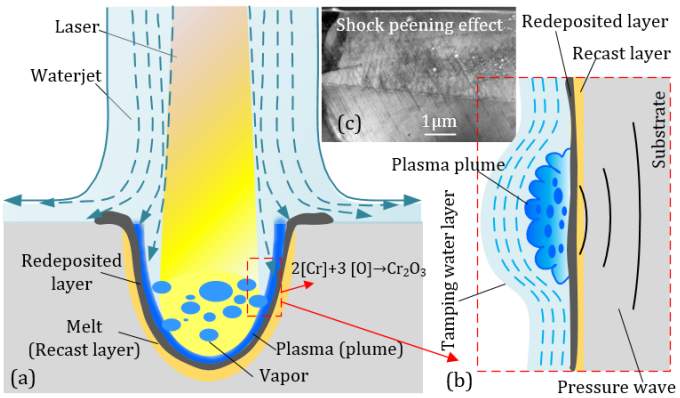


**Fig 8.** (a) Material removal mechanism in WJGL cutting, (b) and (c) secondary shock peening effect on the substrate

## 5. Fatigue performance of WJGL cut Ni-based superalloy

With the elucidation of the formation mechanism of the surface integrity in WLG, there is a need to understand how this influences the functional performance, e.g. fatigue. Fig. 9 (a) presents the fatigue life of WJGL cut Inconel 718, whereby a bench mark, i.e. conventional milled (CM, cutting speed=45 m/min, feed rate=0.25 mm/tooth and depth of cut=0.25 mm) samples.

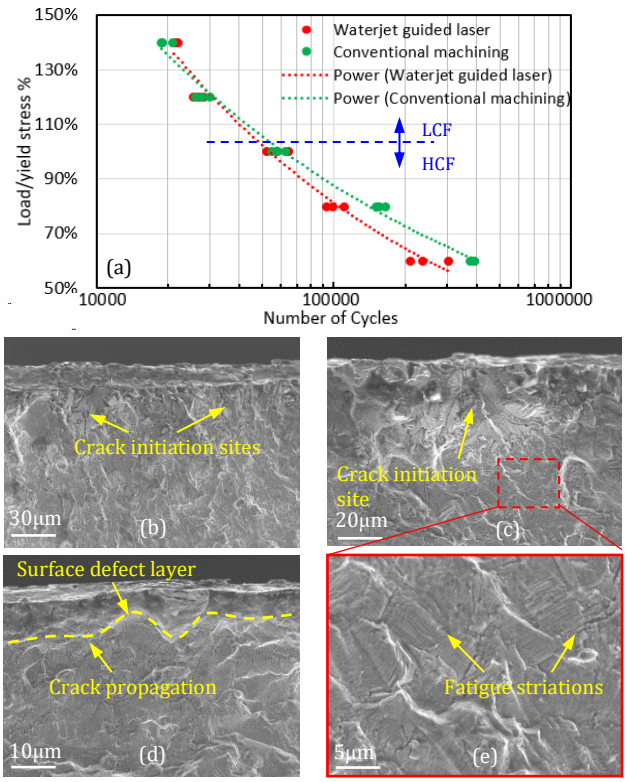


**Fig 9.** (a) Fatigue life and (b)-(e) fractography of WJGL cut Inconel 718

The S-N curve demonstrates that under low cycle fatigue (LCF) the WJGL machined workpieces show similar fatigue life to CM ones while in high cycle fatigue (HCF) the WJGL ones show a marginally shorter life. This manifests that although at HCF the thermally induced tensile residual stresses reduce the fatigue life, at LCF the thick (~8 μm) WL does not have a significant influence on the fatigue life compared to CM sample (~2 μm WL) [7]. This can be attributed to the strengthening effect induced by the MTs aligned in multiple directions through secondary plasma shock peening effect. Nevertheless, from the fracture topography (Fig. 9b and c) WJGL induced WL can generate multiple crack initiation sites throughout the fatigue surface and in the meantime facilitates the crack propagation along this layer (Fig. 9d). The high magnification SEM image of crack initiation site (Fig. 9c) presents high density cleavage plan features which are associated with brittle fracture in WL. However, a high density fatigue striation has also been found surrounding the crack initiation site (Fig. 9e), after a short brittle crack propagation. This indicates that the plasma shock induced MTs can restrain the cleavage growth.

## 6. Conclusion

The material removal mechanism in WJGL cutting is unique due to the combined interaction between laser, waterjet and workpiece. This paper conducted an in-depth investigation of the surface formation mechanism in WJGL cutting of Ni-based superalloy with revealing the role of waterjet in relation to the thermodynamic and kinetic activities of laser ablation process. A white layer has been found on the machined surface with a shallow but high value tensile residual stress from the heating effect. The crystallographic analysis reveals that the white layer is composed of a recast and a redeposited layer. The recast layer represents the solidification of molten material in the forms of recast droplet, layer and spatter. The redeposition is constituted by an amorphous oxide film, which was induced from fast cooling of the explosive plasma plume confined by the waterjet, while a large amount nanocrystallines were also found in this layer solidified from the vaporised mass. A laser shock peening effect has also been demonstrated in this process due to the partial confinement of the plasma plume by the waterjet. The fatigue test presents a short fatigue life in HCF due to high tensile residual stress (1100 MPa) but an eminent performance in LCF due to the strengthening effect of MTs structure. While the cutting parameters selected represent a WJGL roughing stage, further WJGL finishing is also available to achieve improved surface integrity.


## Acknowledgement

This project received funding from Clean Sky 2 JU under EU's Horizon 2020 program (No.754807). The authors also thank the support from Stuart Robertson at Loughborough University.


## References


[1] Rodrigues GC, Duflou JR (2017) Opportunities in laser cutting with direct diode laser configurations. CIRP Annals 66(1): 245-248.
[2] Villerius V et al (2019) Ultrashort pulsed laser ablation of stainless steels. International Journal of Machine Tools and Manufacture 138: 27-35.
[3] Marimuthu S et al. (2019) Water-jet guided laser drilling of SiC reinforced aluminium metal matrix composites. Journal of Composite Materials 53: 3787-3796.
[4] Liu YZ (2020) Coaxial waterjet-assisted laser drilling of film cooling holes in turbine blades. International Journal of Machine Tools and Manufacture 150: 103510.
[5] Xu D et al. (2020). A novel method to continuously map the surface integrity and cutting mechanism transition in various cutting conditions. International Journal of Machine Tools and Manufacture 151, 103529.
[6] Holmberg J et al. (2019) Evaluation of surface integrity after high energy machining with EDM, laser beam machining and abrasive water jet machining of alloy 718. International Journal of Advanced Manufacturing Technology 100: 1575-1591.
[7] Shang Z, et al. (2019) On modelling of laser assisted machining: Forward and inverse problems for heat placement control. International Journal of Machine Tools and Manufacture 138: 36-50.